Robust Stability Assessment of Single-Phase Inverter With Multiparameter Distributions

Yongyang Chen, *Student Member, IEEE*, Shangzhi Pan, *Senior Member, IEEE*, Meng Huang, *Member, IEEE*, Haoran Wang, *Member, IEEE*, Huai Wang, *Senior Member, IEEE*, and Xiaoming Zha, *Member, IEEE*

***Abstract*—Grid-connected inverters inevitably operate under uncertain system parameters. These uncertain parameters such as inductance and capacitance are caused by device aging or uncertain grid conditions. And they will affect the stability margin of the inverter and bring an unstable operation risk even with a well initial design. The existing research articles mainly focus on robust stability analysis and control strategies while ignoring the influence of parameter distributions on operational risk. How to evaluate the instability risk of the inverter under multiparameter distribution is still an open question. In this article, the structured singular value (SSV) method is proposed to evaluate the robust stability of the inverter with multiparameter distributions. The distribution characteristics of uncertain parameters are briefly reviewed. The system model of a single-phase grid-connected inverter is established with the parameter distributions of the system key components. The probability of stable system operation can be quantified by the SSV method. Experiment and case study results verify the correctness and effectiveness of the proposed method.**

***Index Terms*—Robust stability margin, single-phase grid-connected inverter, structured singular value (SSV).**

I. Introduction

As THE utilization capacity of renewable energy increases, the single-phase grid-connected inverter is widely used as the interface between the renewable energy source and the grid [1]. Compared with the *L* filter, the *LCL* filter has better harmonic attenuation ability [2]. However, the *LCL* filter is more sensitive to the parameter variations and increases the resonance hazard of the grid-connected inverter [3]–[6].

A grid-connected inverter is in between the renewable energy and the electric grid. And grid-connected inverters inevitably operate under multiple uncertain parameters. For example, the grid-side impedance parameters would be uncertain due to the different installation locations and working conditions [7]. Furthermore, during the long-term operation, component parameters of the inverter could deviate from their nominal value because of component aging [8]. Typical uncertain parameters that affect the robust stability of the system include controller delay uncertainty [4], grid impedance uncertainty [5]–[10], and *LCL* filter parameter uncertainty [11], [12]. These uncertain parameters will affect the stability margin of the inverter and bring an unstable operation risk even with a well initial design.

The robust stability with parameter uncertainty is a challenge for the inverter [4], [9]. And many control strategies are proposed to improve the robust stability of the grid-connected inverter [9]–[16]. For single-parameter uncertainty, the resonant controller [9] and active damping method [10] are proposed to stabilize the system. For the multiparameter uncertain system, some robust stability methods such as the linear matrix inequalities (LMI) method [11] and H_∞ control synthesis [13]–[15] are proposed to stabilize the system. However, due to the conservativeness of the built-in Lyapunov function and the optimization-based solution method, the LMI and H_∞ methods cannot quantify the robust stability margin of the system [16]. Furthermore, these methods need to determine the maximum perturbation range of the uncertain parameter first, which is difficult to obtain and too conservative in many cases [17]. As the perturbation range of uncertain parameters increases, the solution to LMIs may not exist.

The perturbation range of uncertain parameters in the actual system is difficult to accurately obtain [17]. Even with the help of measuring equipment, the results obtained are only the parameters under fixed working conditions [18]. The distribution characteristic is an effective way to characterize parameter uncertainties [8], [19]. For example, the variance of capacitance is represented by a distribution model [8], and the fluctuation of renewable energy is predicted by distribution characteristics [20], [21]. The robust stability and instability risk of the inverter under multiparameter distributions need to be quantified. For power systems, some probabilistic methods such as Chebyshev's inequality method [22] and stochastic response surface method [23] have been proposed to evaluate the system stability. As for power electronic converters, the nonlinearity of stability analysis makes the application of probabilistic methods difficult. The Monte Carlo method is applied to the stability assessment of inverters [7], [18]. However, the exhaustive method brings a considerable computational burden and often does not get the worst case of the system [17].

Manuscript received June 5, 2021; revised September 16, 2021 and November 13, 2021; accepted November 27, 2021. Date of publication December 9, 2021; date of current version January 19, 2022. This work was supported by the National Natural Science Foundation of China under Grant 51637007. Recommended for publication by Associate Editor F. W. Fuchs. *(Corresponding authors: Meng Huang; Haoran Wang.)*

Yongyang Chen, Shangzhi Pan, Meng Huang, and Xiaoming Zha are with the School of Electrical Engineering and Automation, Wuhan University, Wuhan 430072, China (e-mail: yongyang-chen@whu.edu.cn; shangzhi.pan@whu.edu.cn; meng.huang@whu.edu.cn; xmzha@whu.edu.cn).

Haoran Wang and Huai Wang are with Energy Technology, Aalborg University, 9220 Aalborg, Denmark (e-mail: hao@et.aau.dk; hwa@et.aau.dk).

Color versions of one or more figures in this article are available at https://doi.org/10.1109/TPEL.2021.3133456.

Digital Object Identifier 10.1109/TPEL.2021.3133456

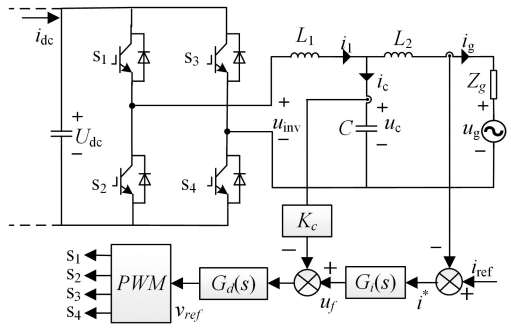

Fig. 1. Structure and control diagram of the single-phase inverter.

The SSV method can effectively analyze the robust stability of a multiparameter uncertain system [24], [25]. Due to the form of the structured uncertainty matrix, the boundaries of the uncertain parameters are related to the SSV, and the system's robust stability margin can be quantified by SSV. In this article, the multiparameter uncertainty model of the inverter is established. According to the definition of SSV, the robust stable parameter domain of the system can be obtained. Combining the robust stable parameter domain and the distributions of uncertain parameters, the system's robust stability and instability risk can be quantified. The proposed method takes the distributions of uncertain parameters into account and avoids the complicated iterative calculation of the Monte Carlo method.

The rest of this article is organized as follows. In Section II, the distribution characteristics of uncertain parameters are briefly reviewed. And the nominal parameter system model is established. In Section III, the uncertainty model is established, and the robust stable parameter domain is obtained through SSV analysis. The robust stability of the system is quantified by combining the robust stable parameter domain with the distributions of uncertain parameters. The Monte Carlo method is also presented in comparison with the proposed SSV method. In Section IV, robust stability assessment results are obtained through the SSV method and Monte Carlo method. The comparison of the two methods explains the assessment conservativeness of the SSV method, and a strategy to reduce conservativeness is proposed. In Section V, a single-phase inverter prototype is established to verify the correctness of the SSV method. Finally, Section VI concludes this article.

II. System Model With Multiple Parameter Uncertainties

The stability of the nominal parameter system is the premise of the system's robust stability. On the basis of the nominal parameter system model, the influence of uncertain parameters on robust stability is analyzed. The structure and control diagram of the single-phase grid-connected inverter are shown in Fig. 1 and the nominal parameters of the inverter are listed in Table I. The control strategy used in this article is output feedback control. The active damping strategy with capacitor current feedback (CCF) is applied to improve the robust stability of the grid-connected inverter [9], [10], and the CCF coefficient is K_c.

TABLE I
Nominal Parameters of the Inverter

System parameters	Symbol	Nominal Value
System capacity	S_{inv}	3000 W
DC voltage	U_{dc}	400 V
Grid voltage (RMS)	U_g	220 V
DC capacitor	C_{dc}	10 mF
Grid-side filter inductance	L_2	0.2 mH
Inverter-side filter inductance	L_1	1 mH
Filter capacitor	C	10 μF
Sampling frequency	F_s	25.6 kHz
Grid resistance	R_g	0.1 Ω
Grid inductance	L_g	0.2 mH
CCF coefficient	K_c	0.1
Controller parameters	K_p/K_r	0.11/11.0

TABLE II
Examples of Parameter Variances of Filter Capacitor and Inductor

Elements	Parameters	Variances	Product number
Filter capacitor	10 μF	±5% - ±10%	KEMET C4AQLBU5100M1XK [27]
Filter inductor	0.9 mH	±15%	Bourns 5709-RC
Filter inductor	1 mH	±20%	EPCOS/TDK B82615B2502M001 [28]

In Fig. 1, L_1, L_2, and C are the nominal parameters of the *LCL* filter, C is the filter capacitor, L_1 is the inverter-side filter inductance, and L_2 is the grid-side filter inductance. The filter capacitor voltage is denoted as u_c. The currents flowing through L_1, L_2, and C are denoted as i_1, i_g, and i_c, respectively. The dc voltage is u_{dc} and the dc current is i_{dc}. The power grid is equivalent to the series of the voltage source u_g and the grid impendence Z_g. The grid impendence Z_g consists of the grid inductance L_g and the grid resistance R_g.

A. Review of Parameter Distributions

The conventional analysis is based on nominal parameters, but the actual inverter inevitably operates under multiple parameter uncertainties. In this section, the possible uncertain parameters during operation are briefly reviewed. And the distribution characteristics of uncertain parameters are given based on mechanism analysis and parameter survey results.

For the filter inductor and capacitor, the survey results of typical parameters on the market are shown in Table II. Due to the limitations of the production process and technical level, component parameters inevitably have deviations. According to the central limit theorem, the distribution of a large number of independent random variables tends to be normal [26]. The normal distribution with an expectation of E and standard deviation of σ is $N(E, \sigma)$.

The probability density function (PDF) is a commonly used representation to reveal the statistical features of samples. Assuming that the distribution of the filter inductor l_1 is a normal

distribution with an expectation of L_1 and standard deviation of σ_1, that is, $l_1 \sim N(L_1, \sigma_1)$. Referring to the PDF of a typical normal distribution [19], the PDF of l_1 is as follows:

$$f_{L1}(l_1) = \frac{1}{\sqrt{2\pi(\sigma_1)^2}} \cdot \exp\left[-\frac{1}{2} \cdot \left(\frac{l_1 - L_1}{\sigma_1}\right)^2\right]. \quad (1)$$

The probability that l_1 is within a certain range is the integral of the PDF

$$P_{L1}(a < l_1 \leq b) = \int_a^b [f_{L1}(l_1)]\, dl_1. \quad (2)$$

The metalized film capacitor is usually used for the *LCL* filter, and the aging process of the filter capacitor is affected by voltage variation and background harmonics. Due to the influence of reactive power, the aging process of the filter capacitor can be characterized by Weibull distribution [8]. According to different reliability requirements, the maximum capacitance loss of the filter capacitor ranges from 5% to 20% [8], [29]. Considering the initial parameter deviation, the maximum perturbation range of the filter capacitor is set from ±20% to ±30%. The Weibull distribution with a scale parameter of η and shape parameter of β is $W_b(\eta, \beta)$.

The PDF of the filter capacitor c is

$$f_C(c) = \frac{\beta}{\eta} \cdot \left(\frac{c}{\eta}\right)^{\beta-1} \cdot \exp\left[-\left(\frac{c}{\eta}\right)^{\beta}\right]. \quad (3)$$

The cumulative density function (CDF) of Weibull distribution is

$$F_C(c) = 1 - \exp\left[-\left(\frac{c}{\eta}\right)^{\beta}\right]. \quad (4)$$

A grid-connected inverter is in between the renewable energy and the electric grid, and the impedance parameter from the grid side would also be uncertain according to the location and work conditions. According to the grid impedance survey results in [7], it is assumed that the grid impedance satisfies a normal distribution, that is, $l_g \sim N[L_g, 5\%L_g]$.

According to the state-space averaging method [30], the transfer function of the inverter is $K_{\mathrm{pwm}} = u_{\mathrm{dc}}/v_{\mathrm{tri}}$, where v_{tri} is the carrier amplitude of the pulse width modulation (PWM) modulation and the default value is 1. Thus, the default value of K_{pwm} is 400. For a single-phase inverter, the fluctuation range of the dc voltage is related to the inverter power fluctuation [31]. Due to photovoltaic power distribution characteristics [21], the distribution of the inverter transfer function is, $k_{\mathrm{pwm}} \sim N[K_{\mathrm{pwm}}, 5\%K_{\mathrm{pwm}}]$.

For the inverter, the delay of the controller is related to the sampling and modulation methods. In the analysis, the sampling period is T_s and the controller delay is between $0.75T_s$ and $1.5T_s$ [32], [33]. According to the above survey results, it is assumed that the distribution of the controller delay is, $t_d \sim N[T_S, 10\%T_S]$.

In addition, there may be other uncertain parameters in actual inverters, and these parameters can be further considered. In the parameter uncertainty study, the uncertain parameters are also characterized as other distribution characteristics, such as: Gauss-Poisson joint distribution [34], Beta distribution [35], and so on. But the stability assessment process of the inverter is the same under different distribution characteristics. The parameter distributions discussed in this section are some examples for the case study.

B. Nominal Parameter System Modeling

According to Fig. 1, the state equations of the *LCL* filter are derived as

$$C\frac{du_c}{dt} = i_1 - i_g \quad (5)$$

$$L_1\frac{di_1}{dt} = u_{\mathrm{inv}} - u_c \quad (6)$$

$$(L_2 + L_g)\frac{di_g}{dt} = u_c - u_g - R_g i_g. \quad (7)$$

The current control adopts a PR regulator, and the transfer function of the PR regulator is

$$G_{\mathrm{i}}(s) = K_p + \frac{2K_r\omega_c s}{s^2 + 2\omega_c s + \omega_0^2} \quad (8)$$

where ω_0 is the fundamental angular frequency, and ω_c is the resonant cutoff frequency. K_p and K_r are the proportional and resonant coefficients.

The controller state variables are defined as x_1, x_2, the state-space equation of the PR regulator is

$$\begin{bmatrix}\dot{x}_1\\ \dot{x}_2\end{bmatrix} = \begin{bmatrix}0 & 1\\ -\omega_0^2 & -2\omega_c\end{bmatrix}\begin{bmatrix}x_1\\ x_2\end{bmatrix} + \begin{bmatrix}2K_c\omega_c\\ -4K_r\omega_c^2\end{bmatrix} i^*. \quad (9)$$

The output of the PR regulator is

$$u_f = K_p i^* + x_1. \quad (10)$$

The controller delay is $G_d(s)$. According to the one-order Taylor expansion, the controller delay can be rewritten as follows [36]:

$$G_d(s) = e^{-sT_d} \approx \frac{1}{1 + sT_d}. \quad (11)$$

The output of the controller delay module $G_d(s)$ is donated as v_{ref}. The state vector is denoted as $x = [u_c, i_1, i_g, x_1, x_2, v_{\mathrm{ref}}]^T$, and the input vector is donated as $u = [u_g, i_{\mathrm{ref}}]^T$. The output of the system is the state variable i_g. Thus, the state-space model of the nominal parameter system is as follows:

$$\begin{bmatrix}y\\ \dot{x}\end{bmatrix} = \begin{bmatrix}O & C\\ B & A\end{bmatrix}\begin{bmatrix}u\\ x\end{bmatrix} \quad (12)$$

where the matrix O has appropriate dimensions and all elements are 0.

The matrices of the nominal parameter system can be expressed as follows:

$$A = \begin{bmatrix} 0 & \frac{1}{C} & -\frac{1}{C} & 0 & 0 & 0\\ -\frac{1}{L_1} & 0 & 0 & 0 & 0 & \frac{K_{\mathrm{pwm}}}{L_1}\\ \frac{1}{L_2+L_g} & 0 & -\frac{R_g}{L_2+L_g} & 0 & 0 & 0\\ 0 & 0 & -2K_r\omega_c & 0 & 1 & 0\\ 0 & 0 & 4K_r\omega_c^2 & -\omega_0^2 & -2\omega_c & 0\\ 0 & -\frac{K_c}{T_d} & \frac{K_c - K_p}{T_d} & \frac{1}{T_d} & 0 & -\frac{1}{T_d} \end{bmatrix} \quad (13)$$

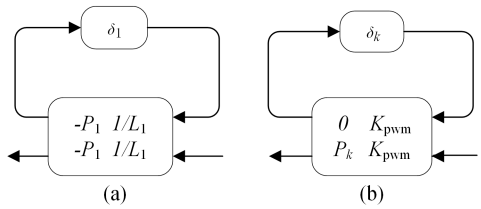

Fig. 2. Upper LFT of uncertain parameters. (a) Inverter-side filter inductance. (b) Inverter transfer function.

$$B=\begin{bmatrix}0\ 0 & -\frac{1}{L_2+L_g} & 0 & 0 & 0\\ 0\ 0 & 0 & 2K_r\omega_c & -4K_r\omega_c^2 & \frac{K_p}{T_d}\end{bmatrix}^{\rm T} \tag{14}$$

$$C=\begin{bmatrix}0\ 0\ 1\ 0\ 0\ 0\end{bmatrix}. \tag{15}$$

The system model with uncertain parameters is derived based on the nominal system model.

III. Proposed Robust Stability Assessment Method

Actual parameters often deviate from their nominal values. Taking the inverter-side filter inductor as an example, the uncertain parameter l_1 consists of the nominal value L_1 and parameter uncertainty. The parameter uncertainty model of l_1 is as follows:

$$l_1{=}L_1\left(1+P_1\delta_1\right) \tag{16}$$

where P_1 is the maximum parameter perturbation percentage of L_1 and the uncertainty $\delta_1{\in}[-1,1]$.

In the state matrix of the nominal system, the inverter-side filter inductor L_1 is in the denominator. Thus

$$\frac{1}{l_1}{=}\frac{1}{L_1}-\frac{P_1\delta_1}{L_1}(1+P_1\delta_1)^{-1}. \tag{17}$$

Considering the dc voltage fluctuation, the inverter transfer function is an uncertain parameter. The uncertain parameter $k_{\rm pwm}$ can be expressed as follows:

$$k_{\rm pwm}{=}K_{\rm pwm}\left(1+P_k\delta_k\right) \tag{18}$$

where P_k is the maximum parameter perturbation percentage of $K_{\rm pwm}$ and the uncertainty $\delta_k{\in}[-1,1]$.

To separate the uncertain part from the known part of the system, the linear fractional transformation (LFT) method is applied to uncertain parameter modeling [25], [37]. The specific LFT method can refer to Appendix A. The upper LFT form of $1/l_1$ is denoted as $F_u\left(M_1,\delta_1\right)$, and the structure of $F_u\left(M_1,\delta_1\right)$ is shown in Fig. 2(a). The coefficient matrix M_1 is expressed as follows:

$$M_1=\begin{bmatrix}-P_1 & 1/L_1\\ -P_1 & 1/L_1\end{bmatrix}. \tag{19}$$

The uncertain parameters of the filter capacitor, the grid-side inductance, and the controller delay are denoted as c, $(l_2{+}l_g)$, and t_d, respectively. The upper LFT forms of $1/c$, $1/\left(l_2{+}l_g\right)$, and $1/t_d$ are $F_u\left(M_c,\delta_{\rm c}\right)$, $F_u\left[M_g,\delta_{\rm g}\right]$, and $F_u\left(M_d,\delta_{\rm d}\right)$, respectively.

The upper LFT form of $k_{\rm pwm}$ is denoted as $F_u\left(M_k,\delta_k\right)$, and the structure of $F_u\left(M_k,\delta_{\rm k}\right)$ is shown in Fig. 2(b). The coefficient matrix M_k is expressed as follows:

$$M_k=\begin{bmatrix}0 & K_{\rm pwm}\\ P_k & K_{\rm pwm}\end{bmatrix}. \tag{20}$$

In (13), there is a division of two uncertain parameters, that is $k_{\rm pwm}/l_1$. The uncertainty is in the form of coprime factor uncertainty, which can also be separated using the LFT method. The multiplication of two LFTs is still an LFT [16], and the upper LFT form of $k_{\rm pwm}/l_1$ can be regarded as the multiplication of $F_u\left(M_1,\delta_1\right)$ and $F_u\left(M_k,\delta_k\right)$. The specific derivation process is also given in Appendix A.

The closed-loop block diagram of the nominal system is shown in Fig. 3(a). The multiparameter uncertainty is taken into consideration based on the nominal parameter system. The uncertain parameters of the single-phase inverter are $l_1, c, {\rm k_{pwm}}$, $(l_2{+}l_g)$, and t_d. With the LFT method, the block diagram of the uncertain system is shown in Fig. 3(b).

As for Fig. 3(b), the parameter uncertainties can be concentrated into the uncertainty matrix $\Delta(s)$ as follows:

$$\Delta\left(s\right)=\mathrm{diag}\left(\delta_c,\delta_1,\delta_k,\delta_g,\delta_d\right). \tag{21}$$

The input vector of the uncertainty matrix $\Delta(s)$ is defined as $y_\Delta=[i_{c\delta},\ u_{1\delta},\ v_{ref\delta},\ u_{g\delta},\ u_{f\delta}]^T$ and the output vector of $\Delta(s)$ is defined as $u_\Delta=[u_{c\delta},\ i_{1\delta},\ u_{inv\delta},\ i_{g\delta},\ u_{d\delta}]^T$. With the LFT method, the extended state-space model is expressed as follows:

$$\begin{bmatrix}y_\Delta\\ \dot{x}\end{bmatrix}=\begin{bmatrix}D_{11} & C_1\\ B_1 & A\end{bmatrix}\begin{bmatrix}u_\Delta\\ x\end{bmatrix}. \tag{22}$$

The state matrix A has been given in (13). The remaining matrices in (22) can be derived through the LFT method, and specific calculations can refer to Appendix A.

The general uncertain system model shown in Fig. 4 is divided into a known parameter matrix $M(s)$ and an uncertainty matrix $\Delta(s)$. The parameters in the matrix $M(s)$ are all known, and $M(s)$ can be obtained through the extended state-space model.

The transfer function matrix $M(s)$ in Fig. 4 can be derived as follows:

$$M\left(s\right)=C_1(sI-A)^{-1}B_1+D_{11} \tag{23}$$

where I is an identity matrix.

For the general uncertain system shown in Fig. 4, the robust stability condition is given by the SSV method [16], [38]. The definition of SSV is as follows:

$$\mu_\Delta\left(M\right)=\frac{1}{\min\left\{\sigma_{\max}\left(\Delta\right)|det\left(I-M\Delta\right)=0,\Delta\mathrm{structured}\right\}} \tag{24}$$

where $\sigma_{\max}(\Delta)$ represents the maximum singular value of the matrix Δ. If there is no uncertainty matrix Δ that makes det($I - M\Delta$) = 0, $\mu_\Delta(M) = 0$.

According to (24), calculating the SSV needs to traverse all the uncertainties and the uncertainty matrix has an infinite variety of values, so the SSV cannot be calculated by definition. Therefore, the upper and lower bounds of SSV are often calculated to determine its range. According to robust control theory, the upper and lower bounds of structured singular value (SSV) can

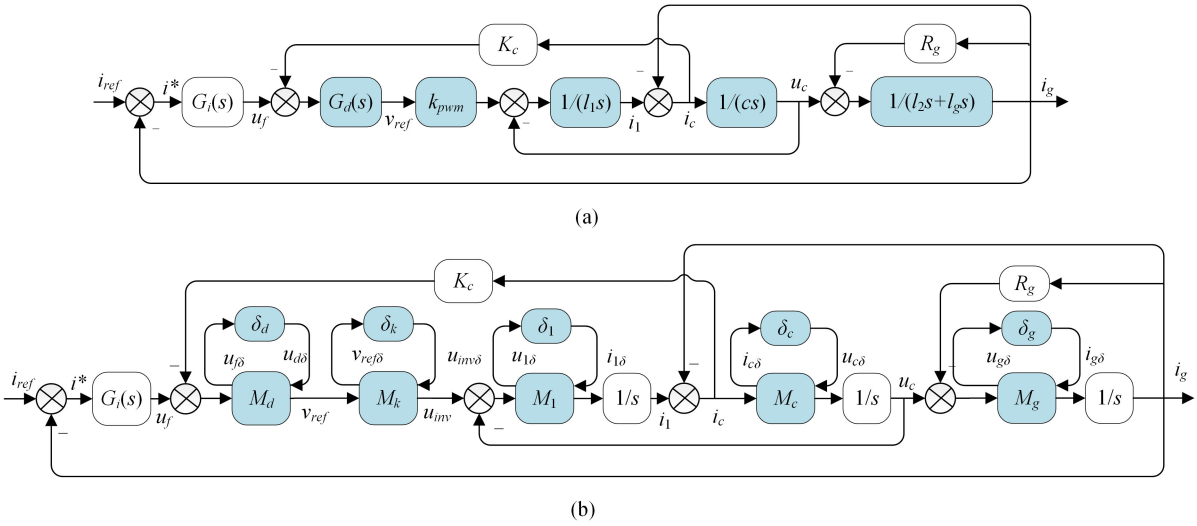

Fig. 3. Closed-loop block diagram of the single-phase inverter. (a) Nominal system. (b) Uncertain system.

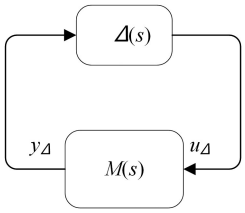

Fig. 4. General uncertain system model.

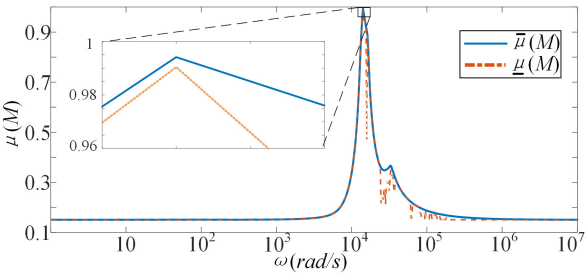

Fig. 5. SSV analysis with the upper and lower bounds.

be determined as follows [16]:

$$\max_{Q} \rho\left(QM\right) \leq \mu_{\Delta}\left(M\right) \leq \inf_{U} \sigma_{\max}\left(UMU^{-1}\right) \tag{25}$$

where Q is a unitary matrix and U is a block diagonal matrix.

It shows that $\mu_{\Delta}(M)$ can be approximated by solving the spectral radius and the maximum singular value. This process can be completed by MATLAB Robust Stability Toolbox. The upper bound of the SSV is denoted as $\bar{\mu}$ and the lower bound of SSV is denoted as $\underline{\mu}$. The default parameter perturbation is set to $\pm 10\%$. The SSV analysis result with the upper and lower bounds is shown in Fig. 5. It can be seen that the upper bound of SSV is 0.995 and the lower bound of SSV is 0.99 in the default case. The difference between the upper and lower bounds does not exceed 1%, and the actual value of SSV can be estimated by the upper and lower bounds. In the following figures, only the upper bound of SSV is shown.

According to the SSV method [16], the SSV analysis can quantify the robust stability margin of the system. The condition for the system's robust stability is as follows:

$$\sigma_{\max}\left(\Delta\left(j\omega\right)\right) \leq \frac{1}{\mu_{\Delta}\left(M\left(j\omega\right)\right)} \forall \omega. \tag{26}$$

As shown in ([21), because the uncertainty matrix Δ is a diagonal matrix composed of parameter uncertainties, the maximum singular value of Δ is determined by the maximum parameter uncertainty. If the SSV of the system is denoted as μ, the robust stability margin is $1/\mu$. Thus, the conditions for the system's robust stability can be derived as follows:

$$\sigma_{\max}\left(\Delta\left(j\omega\right)\right) = \max(\delta_c, \delta_1, \delta_k, \delta_g, \delta_d) \leq \frac{1}{\mu}. \tag{27}$$

The uncertain model of l_1 is shown in (16), and the initial uncertainty of the product perturbation model $\delta \in [-1,1]$. According to the SSV method [16], if μ is less than 1, the system is robust and stable within the maximum parameter perturbation range and the perturbation range of uncertain parameters can be expanded to $1/\mu$ times. Meanwhile, if μ is greater than 1, the maximum parameter perturbation of robust stability is reduced to $1/\mu$ times. In summary, the uncertain parameters need to meet the following conditions to guarantee the system's robust stability

$$\begin{cases} \mathrm{V}: t_d \in \left[T_d\left(1-P_d/\mu\right), T_d\left(1+P_d/\mu\right)\right] \\ \mathrm{W}: k_{\mathrm{pwm}} \in \left[K_{\mathrm{pwm}}\left(1-P_k/\mu\right), K_{\mathrm{pwm}}\left(1+P_k/\mu\right)\right] \\ \mathrm{X}: l_1 \in \left[L_1\left(1-P_1/\mu\right), L_1\left(1+P_1/\mu\right)\right] \\ \mathrm{Y}: c \in \left[C\left(1-P_c/\mu\right), C\left(1+P_c/\mu\right)\right] \\ \mathrm{Z}: \left(l_2+l_g\right) \in \left[\left(L_2+L_g\right)\left(1-P_g/\mu\right)\right. \\ \left.\left(L_2+L_g\right)\left(1+P_g/\mu\right)\right] \end{cases}. \tag{28}$$

According to the review of parameter distributions in Section II, probabilities of events are known. Since the parameter distributions of the independent components are independent, the robust stable probability under corresponding parameter

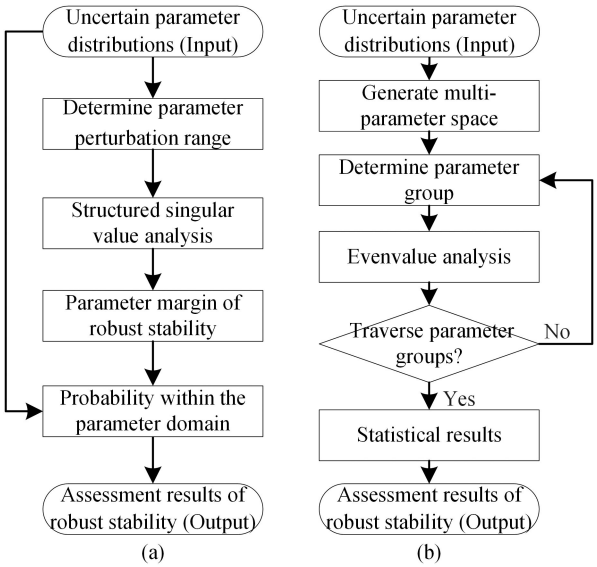

Fig. 6. Robust stability assessment process. (a) SSV method. (b) Monte Carlo method.

distributions is as follows:

$$P_{\mathrm{ssv}}=P\,[\mathrm{V}]\cdot P\,[\mathrm{W}]\cdot P\,[\mathrm{X}]\cdot P\,[\mathrm{Y}]\cdot P\,[\mathrm{Z}]\,. \tag{29}$$

In this section, the SSV method is introduced to assess the robust stable probability of the grid-connected inverter. In practical applications, the uncertain parameters may be one or multiple in Section II.

The robust stability assessment process using the SSV method is shown in Fig. 6(a). First, the perturbation range of the uncertain parameter can be determined according to the parameter distribution. Second, the SSV of the uncertain parameter system can be calculated. Third, the robust stable parameter domain of the system can be obtained. Finally, the assessment result of robust stability is determined by combining uncertain parameter distribution.

In order to compare with the proposed SSV method, this article also presents the Monte Carlo method based on eigenvalue analysis. The robust stability assessment process with the Monte Carlo method is shown in Fig. 6(b). The input of the assessment process is multiparameter distributions and the output is stability probability or instability risk. The specific calculation process of the Monte Carlo method is described in detail in Appendix B.

IV. Case Study

A. Robust Stability Analysis With Single-Parameter Uncertainty

In this section, the results of SSV analysis are compared with that of eigenvalue analysis. The nominal parameters of the system are shown in Table I. For SSV analysis, the uncertain parameters are l_1, l_g, c, and k_{pwm} and the default perturbation range of uncertain parameters is $\pm 10\%$. As for eigenvalue analysis, the default value of the uncertain parameter is 1.1 times the nominal value.

TABLE III
Uncertain Parameter Distribution

	Case 1	Case 2	Case3	Case4	Case5
c	$W_b(C, 7)$	$W_b(C, 7)$	$W_b(C, 7)$	$W_b(C, 10)$	$W_b(C, 10)$
l_1	$N(L_1, 5\%L_1)$	$N(L_1, 5\%L_1)$	$N(L_1, 5\%L_1)$	$N(L_1, 5\%L_1)$	$N(L_1, 5\%L_1)$
l_g	–	--	--	$N(L_g, 5\%L_g)$	$N(L_g, 5\%L_g)$
k_{pwm}	–	--	--	$N(K_{pwm}, 5\%K_{pwm})$	$N(K_{pwm}, 5\%K_{pwm})$
t_d	–	--	--	--	$N(T_d, 10\%T_d)$
P_c	±30%	±30%	±30%	±20%	±20%
P_l	±15%	±20%	±30%	±30%	±30%
P_g	–	--	--	±30%	±30%
P_k	–	--	--	±15%	±15%
P_d	–	--	--	--	±30%

The robust stability analysis results with single-parameter variance are shown in Fig. 7. When the filter capacitor parameter varies, Fig. 7(a) is a part of the eigenvalue loci and Fig. 7(d) is the results of SSV analysis. The direction of the arrow indicates the increase of the filter capacitor C. When the capacitance is 1.1 times the nominal value, the real part of the eigenvalue is about to exceed 0, and the maximum value of SSV is about to exceed 1. Furthermore, the imaginary part of the eigenvalue and the frequency of the maximum SSV are both around 2.5 kHz. When the capacitance increases, the real part of the eigenvalue loci move toward the positive, and the maximum value of SSV increases. The SSV analysis result corresponds to the eigenvalue analysis result. The eigenvalue loci with the variance of the inverter-side filter inductor and the grid inductance are shown in Fig. 7(b) and (c), respectively. And the SSV analysis results are shown in Fig. 7(e) and (f), respectively. The direction of the arrow indicates the increase of the parameter. The analysis results of the two methods can also correspond to each other, which shows the correctness and effectiveness of the SSV analysis.

With single-parameter variance, the eigenvalue method can analyze the stability of the system. However, the robust stability margin of the system cannot be obtained through eigenvalues. The proposed SSV method can quantify the robust stability margin to evaluate the robust stability of the system. Fig. 8 shows the influence of different parameter variations on the SSV. The range of uncertain parameters varies from 0.9 times the nominal value to 1.1 times the nominal value. In this case, the filter capacitor c and the inverter transfer function k_{pwm} have a greater impact on the SSV. Therefore, the filter capacitor and the inverter transfer function are more important parameters for stability in this case.

B. Robust Stability Assessment With Multiparameter Distributions

The parameter distributions and perturbations for the case study are listed in Table III. The distribution characteristics of uncertain parameters correspond to the parameter review in Section II. For a typical normal distribution, more than 99.7% of the parameters are distributed within three times the standard deviation. Thus, the default parameter perturbations are set as

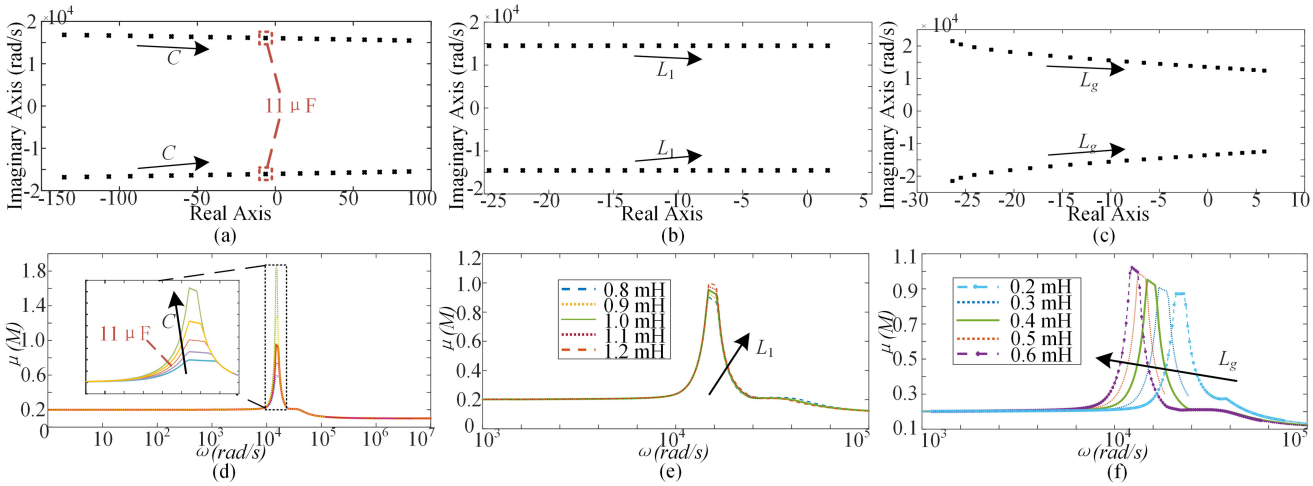

Fig. 7. Robust stability analysis with the nominal parameter change. (a) Eigenvalue loci with C change. (b) Eigenvalue loci with L_1 change. (c) Eigenvalue loci with L_g change. (d) SSV analysis with C change. (e) SSV analysis with L_1 change. (f) SSV analysis with L_g change.

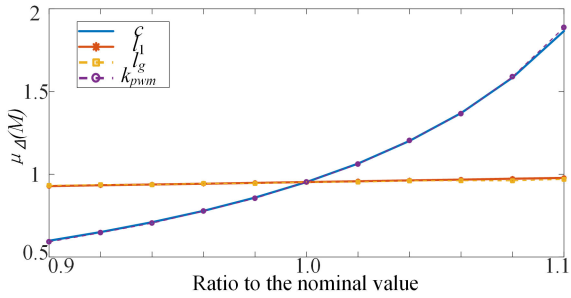

Fig. 8. Influence of parameter variation on the structured singular value.

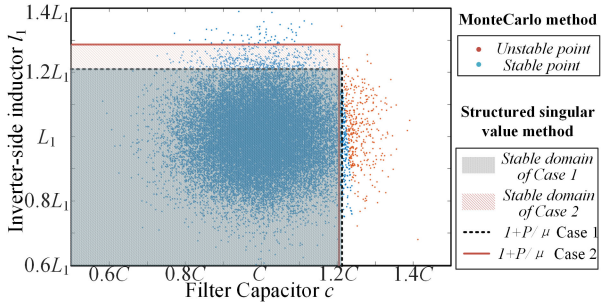

Fig. 9. Comparison of robust stable domain between the SSV method and Monte Carlo method.

TABLE IV
ROBUST STABILITY ASSESSMENT RESULTS

	$\overline{\mu}$	$1/\overline{\mu}$	P_{SSV}	$\underline{\mu}$	$1/\underline{\mu}$	P_{SSV}	P_{MC}
Case 1	1.374	0.728	96.72%	1.336	0.749	97.15%	98.45%
Case 2	1.38	0.725	97.91%	1.35	0.741	98.14%	98.45%
Case 3	1.385	0.722	98.06%	1.37	0.729	98.15%	98.45%
Case4	1.65	0.606	92.38%	1.64	0.610	92.54%	99.38%
Case 5	1.86	0.538	84.17%	1.76	0.568	86.42%	98.96%

three times the standard deviation and the corresponding confidence intervals are 99.7%. Similarly, the confidence interval of the Weibull distribution is also set to exceed 90%. The corresponding robust stability assessment results are shown in Table IV.

In Case 1, Case 2, and Case 3, the uncertain parameter distributions are the same, and the parameter perturbation ranges of the inverter-side inductor l_1 are three times, four times, and six times the standard deviation, respectively. In Table IV, the assessment results with the SSV method are conservative compared with the Monte Carlo method. The reason can be seen from Fig. 9. Fig. 9 shows the robust stable domain of the SSV method and the Monte Carlo method. Since the infinite norm of the uncertainty matrix $\Delta(s)$ is determined by the maximum perturbation, the robust stable domain of the SSV method is a rectangular parameter region. The stable domain of the Monte Carlo method is a set of discrete points formed by each parameter group. Some stable points are located outside the stable domain of the SSV method, which results in the conservativeness of assessment. Compared with Case 1, increasing the perturbation of the grid-side inductance l_1 can reduce the assessment conservativeness of the SSV method in Case 2 and Case 3. That is because the SSV is more sensitive to the variance of the filter capacitor c. With the perturbation increase of l_1, the SSV increases slightly, but the stability domain of the SSV method expands significantly.

In Case 4 and Case 5, the number of uncertain parameters is 4 and 5, respectively. The stable domain of the SSV method is a hypercube in these cases, and the stable domain of the MC method is still a point set. With the increase of uncertain parameters, more and more stable parameter groups are outside the hypercube. Therefore, the assessment conservativeness of the SSV method increases. In Table IV, the assessment result is the stability probability, and the sum of stability probability and instability risk is 1. The assessment results of the instability risk are shown in Fig. 10.

V. EXPERIMENTAL VERIFICATION

To verify the correctness of the SSV analysis, a single-phase grid-connected inverter prototype is established, as shown in

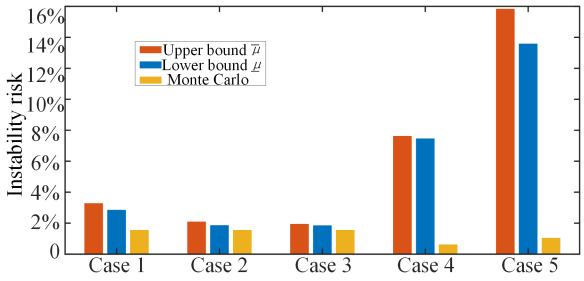

Fig. 10. Instability risk assessment results.

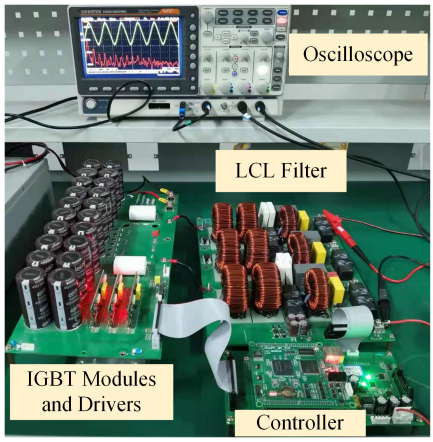

Fig. 11. Single-phase grid-connected inverter prototype.

TABLE V
EXPERIMENT VERIFICATION OF ROBUST STABILITY ASSESSMENT

Parameter groups	L_1/mH	(L_2+L_g) /mH	C/μF	*Experiment Results*	
				Controller A	*Controller B*
Nominal parameter	1.0	0.5	10	P_{SSV}=93.70%	P_{SSV}=77.83%
Group 1	1.020	0.499	9.902	Stable	Stable
Group 2	1.020	0.512	9.902	Stable	Stable
Group 3	1.020	0.505	9.902	Stable	Stable
Group 4	1.020	0.490	9.902	Stable	Stable
Group 5	1.020	0.473	9.902	Stable	Unstable
Group 6	1.024	0.499	9.735	Stable	Stable
Group 7	1.024	0.512	9.735	Stable	Stable
Group 8	1.024	0.505	9.735	Stable	Stable
Group 9	1.024	0.490	9.735	Stable	Stable
Group 10	1.024	0.473	9.735	Stable	Unstable

Fig. 11. In the experiment, the ac grid is emulated by the Chroma programmable AC source 61509, and the grid impedance is connected in series between the ac source and the inverter. The inverter transfer function is $K_{\mathrm{pwm}} = 50$; the rms of grid voltage is $U_g = 25$ V. The sampling frequency in the experiment is 6.4 kHz. The nominal parameters of the *LCL* filter are shown in Table V.

The experimental parameters of the filter are measured under static conditions by ANBAI AT2816A digital bridge. Due to the magnetization characteristics of the inductor, the actual

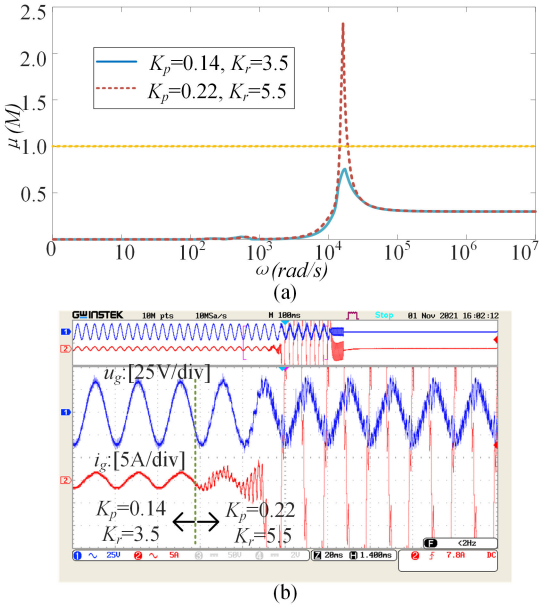

Fig. 12. Experimental verification of SSV analysis. (a) SSV analysis. (b) Experimental result with the controller parameters change.

inductance parameters will change with the magnitude of the current, while the capacitance parameters are basically unchanged. Furthermore, the controller delay is inevitable. The uncertain parameters in the experiment include l_1, l_2, and t_d. According to review of the uncertain parameters in Section II, the parameter perturbations of the inductors are set as $P_1 = 0.3$ and $P_g = 0.3$. The perturbation of the uncertain controller delay is $P_d = 0.3$. The capacitor current feedforward coefficient K_c is 0.04, the proportional coefficient of the PR controller is K_p, and the resonance coefficient is K_r.

A. *Verification of SSV Boundary*

As mentioned in Section III, the boundary of robust stability is whether the maximum value of SSV exceeds 1. The SSV analysis results under different controller parameters are shown in Fig. 12(a). When the controller parameters are $K_p = 0.14$ and $K_r = 3.5$, the SSV analysis result does not exceed 1. After the controller parameters are increased, the maximum value of SSV analysis exceeds 1. The corresponding experimental result with the controller parameters change is shown in Fig. 12(b). When the controller parameters change, the system changes from a stable state to an unstable state. The protection time of the ac source (Chroma 61509) is 0.1 s, so the grid current decreases after five cycles of divergence. In the following two cycles, the controller stops the PWM modulation and the system stops operation. The experimental results are consistent with the SSV analysis, which indicates the correctness of the SSV method.

B. *Verification of Robust Stability Assessment*

Based on the robust stability analysis, the robust stability assessment further considers the parameter distributions. In the subsection, different groups of *LCL* filter parameters are studied.

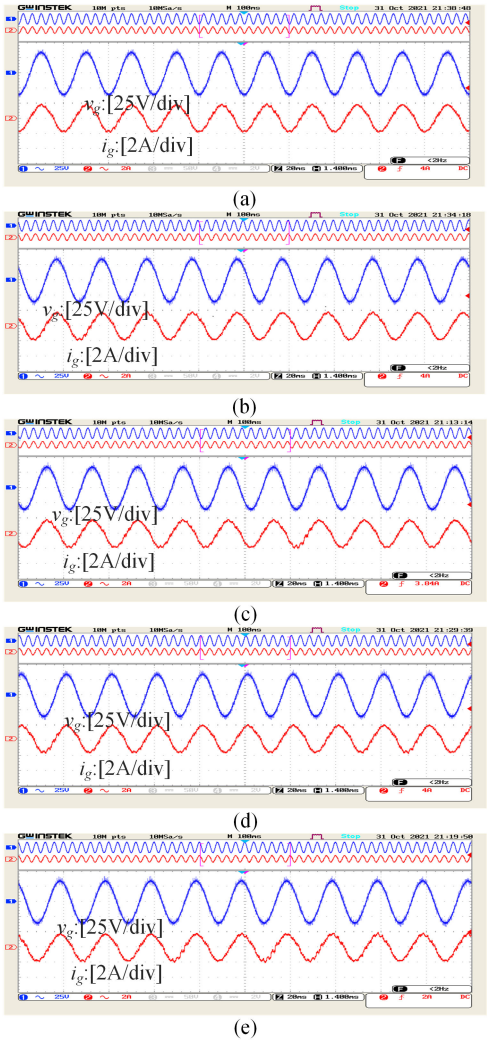

Fig. 13. Experimental results of different parameter groups with controller A. (a) Group 1. (b) Group 2. (c) Group 3. (d) Group 4. (e) Group 5.

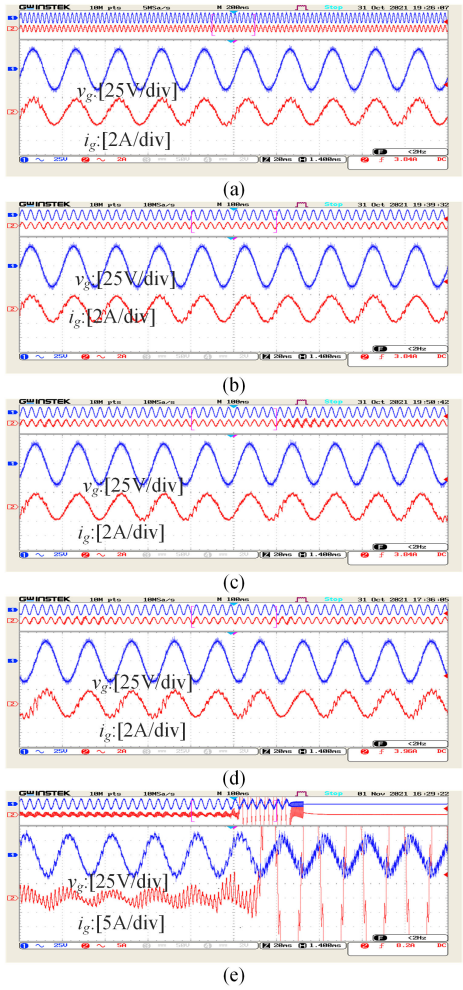

Fig. 14. Experimental results of different parameter groups with controller B. (a) Group 1. (b) Group 2. (c) Group 3. (d) Group 4. (e) Group 5.

The measured values of these *LCL* filter groups are listed in Table V. In the experiment, two controllers are set. Controller A is $K_p = 0.18$ and $K_r = 4.5$, and controller B is $K_p = 0.2$ and $K_r = 5.0$. The experimental results of all groups are recorded in Table V. The experimental results of Group 1 to Group 5 are shown in Figs. 13 and 14. The experimental results with controller A are shown in Fig. 13, and the experimental results with controller B are shown in Fig. 14.

For the experimental condition, the SSV analysis results of controller A and controller B are 1.32 and 1.68, respectively. The distribution characteristics of uncertain parameters are assumed to be normal distributions. The robust stability assessment results of controller A and controller B are 93.7% and 77.83%, respectively. This indicates that both controllers A and B are at risk of robust instability for experimental conditions, and controller B has a higher risk of instability.

The experimental results of the ten groups are all stable for controller A, and the experimental results of groups 5 and 10 are unstable for controller B. The proportions of stable experimental results are 100% and 80%, respectively. The error between the assessment results and the statistical results does not exceed 7%, which verifies the correctness and effectiveness of the proposed robust stability assessment method.

Unlike the relatively extreme operating conditions in Section V-A, the variance of filter parameters in Section V-B has a significant impact on robust stability. Although the maximum value of SSV analysis exceeds 1, the experimental results of some groups are still stable. This is because the uncertain parameters in the experiment are not on the perturbation boundaries. Meanwhile, the assessment results are consistent with the experimental results. This also illustrates the significance of robust stability assessment. According to different requirements, the robust stability of the inverter can be designed to different levels. The robust stability assessment result of controller A is 93.7%, which is acceptable under general conditions. And this is also proved by the experimental results.

VI. Conclusion

In this article, a robust stability assessment method is proposed to quantify the inverter's operational risk with

multi-parameter distributions. The system model with multiparameter uncertainties is established using LFT and the robust stable parameter domain is obtained through SSV analysis. Moreover, robust stability assessment results are obtained and compared through the SSV method and Monte Carlo method. Case study and experimental results verify the correctness and effectiveness of the proposed method. This comparative study of the two methods conducts the following conclusions.

1) According to the components' parameter distributions, the robust stability assessment of the multiparameter uncertain system can be performed through the SSV method. Therefore, the complicated iterative calculation of the Monte Carlo method can be avoided;
2) With two uncertain parameters, the robust stability assessment results of the SSV method are close to that of the Monte Carlo method (difference lower than 2% in Table IV). However, the SSV method would be conservative when more parameters are considered simultaneously. And the main source of conservativeness is the constraint of the uncertainty matrix;
3) The instability trend can be predicted if more uncertain parameters are considered. And the SSV assessment conservativeness can be reduced with a reasonable choice of parameter perturbation.

APPENDIX A

This section describes the situation when two LFTs are connected. $F_u\,(M,\,\Delta_1)$ is the upper LFT form of coefficient matrix M and uncertainty matrix Δ_1.

$$F_u\left(M,\Delta_1\right)=M_{22}+M_{21}\Delta_1(I-M_{11}\Delta_1)^{-1}M_{12}. \quad \text{(A1.1)}$$

The corresponding coefficient matrix M is as follows:

$$M=\begin{bmatrix}M_{11} & M_{12}\\ M_{21} & M_{22}\end{bmatrix}. \quad \text{(A1.2)}$$

Similarly, $F_u\,(Q,\,\Delta_2)$ is the upper LFT form of coefficient matrix Q and uncertainty matrix Δ_2. The result of multiplying two LFTs is still an LFT [16].

$$F_u\left(N,\Delta\right)=F_u\left(M,\Delta_1\right)\cdot F_u\left(Q,\Delta_2\right). \quad \text{(A1.3)}$$

The corresponding coefficient matrix and uncertainty matrix are as follows:

$$N=\left[\begin{array}{cc:c}M_{11} & M_{12}Q_{21} & M_{12}Q_{22}\\ 0 & M_{11} & Q_{12}\\ \hdashline M_{21} & M_{22}Q_{21} & M_{22}Q_{22}\end{array}\right] \quad \text{(A1.4)}$$

$$\Delta=\begin{bmatrix}\Delta_1 & 0\\ 0 & \Delta_2\end{bmatrix}. \quad \text{(A1.5)}$$

With the LFT method, the corresponding matrices in (22) can be derived as follows:

$$B_1=\begin{bmatrix}-P_c & 0 & 0 & 0 & 0\\ 0 & -P_1 & P_k/L_1 & 0 & 0\\ 0 & 0 & 0 & -P_g & 0\\ 0 & 0 & 0 & 0 & 0\\ 0 & 0 & 0 & 0 & 0\\ 0 & 0 & 0 & 0 & -P_d\end{bmatrix} \quad \text{(A1.6)}$$

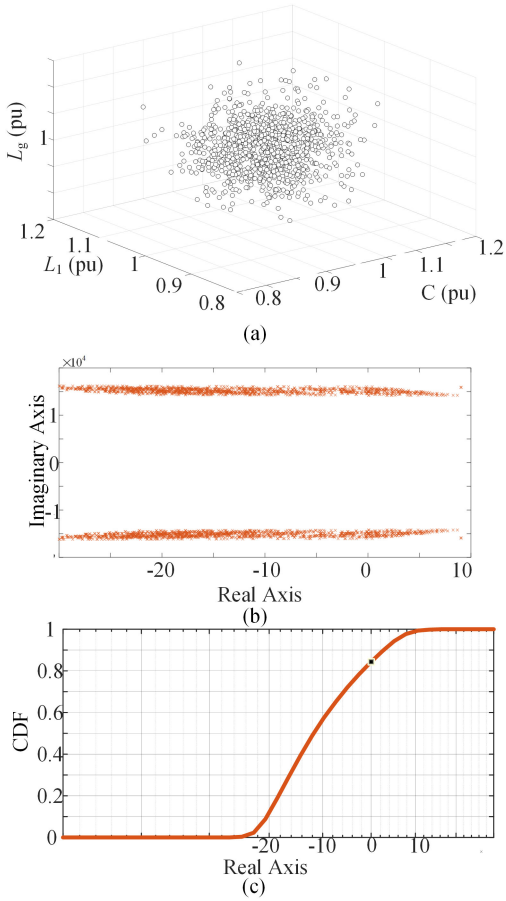

Fig. 15. Robust stability assessment schematic diagram of the Monte Carlo method. (a) Multiparameter space. (b) Eigenvalue analysis results. (c) Statistical results (CDF).

$$C_1=\begin{bmatrix}0 & \frac{1}{C} & -\frac{1}{C} & 0 & 0 & 0\\ -\frac{1}{L_1} & 0 & 0 & 0 & 0 & \frac{K_{\rm pwm}}{L_1}\\ 0 & 0 & 0 & 0 & 0 & K_{\rm pwm}\\ \frac{1}{L_2+L_g} & 0 & -\frac{R_g}{L_2+L_g} & 0 & 0 & 0\\ 0 & -\frac{K_c}{T_d} & \frac{K_c-K_p}{T_d} & \frac{1}{T_d} & 0 & -\frac{1}{T_d}\end{bmatrix} \quad \text{(A1.7)}$$

$$D_{11}=\begin{bmatrix}-P_c & 0 & 0 & 0 & 0\\ 0 & -P_1 & P_k/L_1 & 0 & 0\\ 0 & 0 & -P_1 & 0 & 0\\ 0 & 0 & 0 & -P_g & 0\\ 0 & 0 & 0 & 0 & -P_d\end{bmatrix}. \quad \text{(A1.8)}$$

APPENDIX B

The basic robust stability assessment flow of the Monte Carlo method can be summarized as follows. Taking the distribution of inductance and capacitance as an example, the schematic diagram of the Monte Carlo method is shown in Fig. 15. First, according to the aforementioned parameter distributions, a large number of parameter groups are generated. These parameter groups constitute the multiparameter space, and the multiparameter space is shown in Fig. 15(a). The number of parameter groups is N_P. Subsequently, the corresponding eigenvalues of each parameter group are calculated through the nominal system

model, and the eigenvalues of the parameter groups are shown in Fig. 15(b). Finally, the number of parameter groups with the real part of the eigenvalue less than 0 is obtained by statistics. And the statistical number of eligible parameter groups is recorded as Num. The statistical result is shown in Fig. 15(c). Thus, the stability probability under multiparameter distributions can be obtained as follows:

$$P_{\mathrm{MC}} = \frac{\mathrm{Num}}{N_P}. \tag{A2.1}$$

The Monte Carlo method in this article is an extension of the conventional eigenvalue loci. The eigenvalue analysis is based on the nominal parameter system model, which is given in (12).

REFERENCES

[1] F. Blaabjerg, R. Teodorescu, M. Liserre, and A. V. Timbus, "Overview of control and grid synchronization for distributed power generation systems," *IEEE Trans. Ind. Electron.*, vol. 53, no. 5, pp. 1398–1409, Oct. 2006.

[2] X. Zhang, L. Tan, J. Xian, H. Zhang, Z. Ma, and J. Kang, "Direct grid side current model predictive control for grid-connected inverter with *LCL* filter," *IET Power Electron.*, vol. 11, no. 15, pp. 2450–2460, Dec. 2018.

[3] M. Lu, X. Wang, P. C. Loh, and F. Blaabjerg, "Resonance interaction of multiparallel grid-connected inverterswith *LCL* filter," *IEEE Trans. Power Electron.*, vol. 32, no. 2, pp. 894–899, Feb. 2017.

[4] D. Pan, X. Ruan, C. Bao, W. Li, and X. Wang, "Capacitor-current- feedback active damping with reduced computation delay for improving robustness of *LCL*-type grid-connected inverter," *IEEE Trans. Power Electron.*, vol. 29, no. 7, pp. 3414–3427, Jul. 2014.

[5] M. Liserre, R. Teodorescu, and F. Blaabjerg, "Stability of photovoltaic and wind turbine grid-connected inverters for a large set of grid impedance values," *IEEE Trans. Power Electron.*, vol. 21, no. 1, pp. 263–272, Jan. 2006.

[6] X. Zhou, J. Fan, and A. Q. Huang, "High-frequency resonance mitigation for plug-in hybrid electric vehicles' integration with a wide range of grid conditions," *IEEE Trans. Power Electron.*, vol. 27, no. 11, pp. 4459–4471, Nov. 2012.

[7] E. Kaufhold, J. Meyer, S. Muller, and P. Schegner, "Probabilistic stability analysis for commercial low power inverters based on measured grid impedances," in *Proc. Int. Conf. Power Energy Syst.*, Perth, WA, Australia, 2019, pp. 1–6.

[8] D. Zhou, H. Wang, and F. Blaabjerg, "Reactive power impacts on *LCL* filter capacitor lifetime in grid-connected inverter," *IEEE Open J. Power Electron.*, vol. 1, pp. 139–148, May 2020, doi: 10.1109/OJPEL.2020.2992279.

[9] M. Lu, A. Al-Durra, S. M. Muyeen, S. Leng, P. C. Loh, and F. Blaabjerg, "Benchmarking of stability and robustness against grid impedance variation for *LCL*-filtered grid-interfacing inverters," *IEEE Trans. Power Electron.*, vol. 33, no. 10, pp. 9033–9046, Oct. 2018.

[10] Y. He, X. Wang, X. Ruan, D. Pan, and K. Qin, "Hybrid active damping combining capacitor current feedback and point of common coupling voltage feedforward for *LCL*-type grid-connected inverter," *IEEE Trans. Power Electron.,* vol. 36, no. 2, pp. 2373–2383, Feb. 2021.

[11] C. R. D. Osorio, G. G. Koch, H. Pinheiro, R. C. L. F. Oliveira, and V. F. Montagner, "Robust current control of grid-tied inverters affected by *LCL* filter soft-saturation," *IEEE Trans. Ind. Electron.*, vol. 67, no. 8, pp. 6550–6561, Aug. 2020.

[12] T. Wu, M. Misra, Y. Jhang, Y. Huang, and L. Lin, "Direct digital control of single-phase grid-connected inverters with *LCL* filter based on inductance estimation model," *IEEE Trans. Power Electron.*, vol. 34, no. 2, pp. 1851–1862, Feb. 2019.

[13] L. Huang, H. Xin, and F. Dorfler, "H_∞-control of grid-connected converters: Design, objectives and decentralized stability certificates," *IEEE Trans. Smart Grid*, vol. 11, no. 5, pp. 3805–3816, Sep. 2020.

[14] X. Huang *et al.*, "Robust current control of grid-tied inverters for renewable energy integration under non-ideal grid conditions," *IEEE Trans. Sustain. Energy*, vol. 11, no. 1, pp. 477–488, Jan. 2020.

[15] L. Li, G. Pei, J. Liu, P. Du, L. Pei, and C. Zhong, "2-DOF robust H_∞ control for permanent magnet synchronous motor with disturbance observer," *IEEE Trans. Power Electron.*, vol. 36, no. 3, pp. 3462–3472, Mar. 2021.

[16] K. Zhou, J. Doyle, and K. Glover, *Robust and Optimal Control*. Englewood Cliffs, NJ, USA: Prentice-Hall, 1996.

[17] M. Ferber, A. Korniienko, G. Scorletti, C. Vollaire, F. Morel, and L. Krahenbuhl, "Systematic LFT derivation of uncertain electrical circuits for the worst-case tolerance analysis," *IEEE Trans. Electromagn. Compat.,* vol. 57, no. 5, pp. 937–946, Oct. 2015.

[18] Z. M. Ye, P. K. Jain, and P. C. Sen, "Investigation on uncertainty of resonant inverter system using multiple frequency modeling and Monte Carlo simulation," in *Proc. Int. Telecommun. Energy Conf.*, Chicago, IL, USA, 2004, pp. 274–281.

[19] K. Ma, J. Lin, and Y. Zhu, "Statistical characterization for loss distributions of power semiconductor devices," *IEEE Trans. Power Electron.*, vol. 36, no. 7, pp. 7384–7388, Jul. 2021.

[20] E. B. Ssekulima, M. B. Anwar, A. Al Hinai, and M. S. El Moursi, "Wind speed and solar irradiance forecasting techniques for enhanced renewable energy integration with the grid: A review," *IET Renewable. Power Gener.*, vol. 10, no. 7, pp. 885–989, 2016.

[21] M. Fan, V. Vittal, G. T. Heydt, and R. Ayyanar, "Probabilistic power flow studies for transmission systems with photovoltaic generation using cumulants," *IEEE Trans. Power Syst.*, vol. 27, no. 4, pp. 2251–2261, Nov. 2012.

[22] K. Dehghanpour, Y. Yuan, F. Bu, and Z. Wang, "Statistical modeling of networked solar resources for assessing and mitigating risk of interdependent inverter tripping events in distribution grids," *IEEE Trans. Power Syst.*, vol. 35, no. 5, pp. 3835–3846, Sep. 2020.

[23] E. Haesen, C. Bastiaensen, J. Driesen, and R. Belmans, "A probabilistic formulation of load margins in power systems with stochastic generation," *IEEE Trans. Power Syst.*, vol. 24, no. 2, pp. 951–958, May 2009.

[24] R. Rosso, J. Cassoli, G. Buticchi, S. Engelken, and M. Liserre, "Robust stability analysis of *LCL* filter based synchronverter under different grid conditions," *IEEE Trans. Power Electron.*, vol. 34, no. 6, pp. 5842–5853, Jun. 2019.

[25] S. Sumsurooah, M. Odavic, S. Bozhko, and D. Boroyevich, "Robust stability analysis of a DC/DC buck converter under multiple parametric uncertainties," *IEEE Trans. Power Electron.*, vol. 33, no. 6, pp. 5426–5441, Jun. 2018.

[26] Q. Sun, Y.Z. Tang, J. Feng, and T.D. Jin, "Reliability assessment of metallized film capacitors using reduced degradation test sample," *Qual. Rel. Eng. Int.*, vol. 29, no. 2, pp. 259–265, 2013.

[27] KEMET, "Printed circuit board mount power film capacitors [EB/OL]," 2020, Accessed: Jun. 3, 2021. [Online]. Available: https://www.mouser.cn/datasheet/2/212/1/KEM_F3125_C4AQ_M-1947381.pdf

[28] TDK, "Ring core chokes with iron powder core [EB/OL]," 2012, Accessed: Sep. 23, 2020. [Online]. Available: https://product.tdk.com/info/en/documents/data-sheet/30/db/ind_2008/b82615.pdf

[29] Z. Li *et al.*, "Lifetime prediction of metallized film capacitors based on capacitance loss," *IEEE Trans. Plasma Sci.*, vol. 41, no. 5, pp. 1313–1318, May 2013.

[30] R. D. Middlebrook and S. Cuk, "A general unified approach to modelling switching-converter power stages," in *Proc. IEEE Power Electron. Specialists Conf.*, Cleveland, OH, USA, 1976, pp. 18–34.

[31] D. Zhou, Y. Song, Y. Liu, and F. Blaabjerg, "Mission profile based reliability evaluation of capacitor banks in wind power converters," *IEEE Trans. Power Electron.*, vol. 34, no. 5, pp. 4665–4677, May 2019.

[32] W. Tang, K. Ma, and Y. Song, "Critical damping ratio to ensure design efficiency and stability of *LCL* filters," *IEEE Trans. Power Electron.*, vol. 36, no. 1, pp. 315–325, Jan. 2021.

[33] D. G. Holmes, T. A. Lipo, B. P. McGrath, and W. Y. Kong, "Optimized design of stationary frame three phase AC current regulators," *IEEE Trans. Power Electron.*, vol. 24, no. 11, pp. 2417–2426, Nov. 2009.

[34] Q. Sun, J. Zhou, Z. Zhong, J. Zhao, and X. Duan, "Gauss-Poisson joint distribution model for degradation failure," *IEEE Trans. Plasma Sci.*, vol. 32, no. 5, pp. 1864–1868, Oct. 2004.

[35] H. Bludszuweit, J. A. Dominguez-Navarro, and A. Llombart, "Statistical analysis of wind power forecast error," *IEEE Trans. Power Syst.*, vol. 23, no. 3, pp. 983–991, Aug. 2008.

[36] W. Ma, Y. Guan, B. Zhang, and L. Wu, "Active disturbance rejection control based single current feedback resonance damping strategy for *LCL*-type grid-connected inverter," *IEEE Trans. Energy Convers.*, vol. 36, no. 1, pp. 48–62, Mar. 2021.

[37] W. Lu, K. Zhou, and J. C. Doyle, "Stabilization of uncertain linear systems: An LFT approach," *IEEE Trans. Autom. Control*, vol. 41, no. 1, pp. 50–65, Jan. 1996.

[38] A. Packard and J. Doyle, "The complex structured singular value," *Automatica*, vol. 29, no. 1, pp. 71–109, 1993.

Yongyang Chen (Student Member, IEEE) was born in Hefei, Anhui Province, China, in 1996. He received the B.Eng. degree in electrical engineering in 2017 from Wuhan University, Wuhan, China, where he is currently working toward the Ph.D. degree.

His main research interests include the modular multilevel converter and robustness analysis of power converters.

Shangzhi Pan (Senior Member, IEEE) received the B.Sc. and M.Sc. degrees in electrical engineering from Zhejiang University, Hangzhou, China, in 1998 and 2001, respectively, and the Ph.D. degree from Queen's University, Kingston, ON, Canada, in 2008.

In 2018, he joined the College of Electrical Engineering, Wuhan University, Wuhan, China, where he is currently a Professor. He has been Adjunct Faculty with Queen's Center of Energy and Power Electronics Applied Research Laboratory (ePOWER), Kingston, ON, Canada, since 2014. Previously, he was the VP of Research and Development with SPARQ Systems, a Queen's spun-off photovoltaic microinverter company till 2010. He was a Senior Research Engineer with Queen's University from 2008 to 2013. His research interests include digital control techniques for power converters, grid-connected inverters, voltage regulators for computing systems, power converters for renewable energy sources, and power converters for electric vehicles.

Meng Huang (Member, IEEE) received the B.Eng. and M.Eng. degrees from the Huazhong University of Science and Technology, Wuhan, China, in 2006 and 2008, respectively, and the Ph.D. degree from Hong Kong Polytechnic University, Hong Kong, in 2013.

He is currently an Associate Professor with the School of Electrical Engineering and Automation, Wuhan University, Wuhan, China. His research interests include nonlinear analysis of power converters and power electronics reliability.

Dr. Huang is a Corresponding Guest Editor for the *IEEE Journal on Emerging and Selected Topics in Circuits and Systems*, and the Guest Associate Editor for the *IEEE Journal of Emerging and Selected Topics of Power Electronics*. He was the recipient of the Best Paper Award of the IEEE TRANSACTIONS ON POWER ELECTRONICS in 2016 and the Excellent Paper Award of the *CSEE Journal of Power and Energy Systems* in 2020.

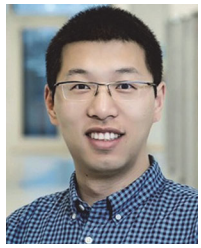

Haoran Wang (Member, IEEE) received the B.S. and M.S. degrees in control science and engineering from the Wuhan University of Technology, Wuhan, China, in 2012 and 2015, respectively, and the Ph.D. degree in energy technology from the Center of Reliable Power Electronics (CORPE), Aalborg University, Aalborg, Denmark.

From 2013 to 2014, he was a Research Assistant with the Department of Electrical Engineering, Tsinghua University, Beijing, China. He was a Visiting Scientist with ETH Zurich, Zurich, Switzerland, from 2017 to 2018, with Kiel University, Kiel, Germany, and Danfoss Drives A/S, Gråsten, Denmark, in 2019. From 2019 to 2021, he was an Assistant Professor with Aalborg University. His research interests include reliability of electrical and electronic components and systems, multiobjective life-cycle performance optimization of power electronic systems, and reliable clean energy control systems.

Huai Wang (Senior Member, IEEE) received the B.E. degree in electrical engineering from the Huazhong University of Science and Technology, Wuhan, China, in 2007, and the Ph.D. degree in power electronics from the City University of Hong Kong, Hong Kong, in 2012.

He is currently a Professor with AAU Energy, Aalborg University, Aalborg, Denmark, where he leads the Group of Reliability of Power Electronic Converters (ReliaPEC) and the mission on Digital Transformation and AI. He was a Visiting Scientist with ETH Zurich, Zurich, Switzerland, from August to September 2014, and with the Massachusetts Institute of Technology (MIT), Cambridge, MA, USA, from September to November 2013. He was with ABB Corporate Research Center, Baden-Dättwil, Switzerland, in 2009. His research interests include the fundamental challenges in modeling and validation of power electronic component failure mechanisms and application issues in system level predictability, condition monitoring, circuit architecture, and robustness design.

Dr. Wang is currently the Chair of IEEE PELS/IAS/IES Chapter in Denmark. He is an Associate Editor for *IET Electronics Letters, IEEE Journal of Emerging and Selected Topics in Power Electronics*, and IEEE TRANSACTIONS ON POWER ELECTRONICS. He was the recipient of the Richard M. Bass Outstanding Young Power Electronics Engineer Award from the IEEE Power Electronics Society in 2016, and the Green Talents Award from the German Federal Ministry of Education and Research in 2014.

Xiaoming Zha (Member, IEEE) was born in Huaining, Anhui Province, China, in 1967. He received the B.S., M.S., and Ph.D. degrees in electrical engineering from Wuhan University, Wuhan, China, in 1989, 1992, and 2001, respectively.

He was a Postdoctoral Fellow with the University of Alberta, Edmonton, AB, Canada from 2001 to 2003. He has been a Faculty Member with Wuhan University since 1992, and became a Professor in 2003. He is currently the Deputy Dean with the School of Electrical Engineering, Wuhan University. His research interests include power electronic converter, the application of power electronics in smart grid and renewable energy generation, the analysis and control of microgrid, the analysis and control of power quality, and frequency control of high-voltage high-power electric motors.